Desalination and Water Treatment
www.deswater.com

doi: 10.1080/19443994.2014.979441

57 (2016) 933–948
January

Taylor & Francis
Taylor & Francis Group

Kinetic and equilibrium study of selenium removal from wastewater in mag-molecular process

Yaser Nabavi Larimi[a,*], Mohammad Hassan Mallah[b], Mohammad Ali Moosavian[c], Jaber Safdari[d]

[a]*School of Chemical Engineering, College of Engineering, University of Tehran, P.O. 47771-16796, Tehran, Iran, Tel. +98 124 3352512; Fax: +98 21 77682113; email: nabavi.yaser@ut.ac.ir*
[b]*Nuclear Fuel Cycle Research School, Nuclear Science & Technology Research Institute, Atomic Energy Organization of Iran, End of North Karegar Ave., P.O. Box 14395-836, Tehran, Iran, Tel. +98 21 82064483; Fax: +98 21 88221113; email: mmallah@aeoi.org.ir*
[c]*Oil & Gas Center of Excellency, School of Chemical Engineering, College of Engineering, University of Tehran, P.O. Box 11365-4563, Tehran, Iran, Tel. +98 912 5333244; email: moosavian@ut.ac.ir*
[d]*Nuclear Fuel Cycle Research School, Nuclear Science & Technology Research Institute, Atomic Energy Organization of Iran, End of North Karegar Ave., P.O. Box 11365-8486, Tehran, Iran, Tel. +98 21 82063569; Fax: +98 21 88221333; email: jsafdari@aeoi.org.ir*

Received 27 December 2013; Accepted 7 October 2014

ABSTRACT

In the present study, a mag-molecule was fabricated by functionalizing of silica-coated magnetite nanoparticles (MNPs) with 3-aminopropyl triethoxysilane (APTES). The amine functional group on surface of the particles was detected using Fourier transmission infrared spectroscopy technique. The morphology and dispersion of the functionalized magnetite nanoparticles (FMNPs) were observed through SEM images. The X-ray diffraction pattern illustrated the cubic crystal structure of MNPs with 28.79 nm of diameter which was almost identical with SEM images. The kinetic of adsorption was studied and pseudo-second-order represented the best fitting to the experimental data. In addition, chemical adsorption for MNPs and physical adsorption for FMNPs were diagnosed applying the Elovich model. The Freundlich model showed a better result for MNPs, which demonstrates a multilayer adsorption on heterogeneous surface, while the Langmuir model was well fitted to FMNPs data, which indicates a homogeneous adsorption at one layer. Continuous system was performed in the fixed-bed column and the obtained results showed the efficiency of continuous system in selenium (Se) removal. The breakthrough curves were provided in three different flow rates and two bed depths and the results showed that the Thomas model can be a promising model for prediction of column performance. The Yoon–Nelson model also represented an acceptable conformation to experimental data. The time required to reach outlet concentration to 50% of initial concentration was calculated by Yoon–Nelson model, and the results were found to be in agreement with the experiments.

Keywords: Mag-molecular process; Functionalized magnetite nanoparticles; Kinetic and equilibrium study; Fixed-bed column

*Corresponding author.

1. Introduction

Nanoparticles own special physical and chemical properties which make these materials useful for different applications. Among the nanoparticles, magnetic nanoparticles were in center of attention due to their super paramagnetic effect and simple way of detection and separation [1–3]. These magnetic nanoparticles can have many biological and medical uses, including cancer cell detection by magnetic resonance imaging [4], tumor extermination by heating, hyperthermia [5], cancer cell separation [6], and drug delivery [7,8]. These nanoparticles could be also used in chemical engineering processes, such as catalytic reaction [9–11] and adsorption process [12–16]. These nanoparticles are used in the mag-molecular process which is defined as a process in which magnetic particles can be separated from liquid phase by an external magnetic field. The process involves four main step, adsorption, magnetic filtration, backwashing, and regeneration of adsorbent. Considering this definition, mag-molecules are surface-modified magnetic nanoparticles used for different goals. In this study, mag-molecules were prepared by functionalization of silica-coated nanoparticles with amine group (FMNPs) and were used for selenium adsorption. The silica coating on magnetic core has some advantages as follow: silica is an inactive material which does not participate in chemical reactions and that makes the mag-molecule more stable in acidic solution. It reduces conductivity and coagulation of core particles. It also increases the colloidal properties of nanoparticles.

Selenium is needed for human's health and should be received in daily diet in a range of 40–400 ($\mu g\ d^{-1}$). Lack of selenium could cause cardiovascular, muscle, and liver disease. Receiving it more than 400 ($\mu g\ d^{-1}$) also causes gastrointestinal disorders, hair loss, sloughing of nails, fatigue, irritability, and neurological damage [17,18]. This element has several radioactive isotopes such as ^{79}Se, with 3.27×10^5 years of half-life time [19]. So, even the trace amount of this element should be removed from wastewater.

Several methods have been applied to prevent the entrance of Se in the environment. Due to anionic nature of Se in water, most of these adsorption processes were performed at very low pH. Wasewar et al. [20] adsorbed Se(IV) onto granular and powdered activated carbon. The optimum adsorbent dosages were found to be 10 and 8 $g\ L^{-1}$ for granules and powder, respectively. Maximum adsorption capacities were attained 9.28 and 11.92 $\mu g\ L^{-1}$ for granules and powder, respectively. They used membrane filtering for the separation of saturated sorbent from the solution. Meng et al. [21] used elemental iron for removal of selenocyanate with concentration of 5 $mg\ L^{-1}$. Only 66% removal was attained after 2 h with iron content of 15 $g\ L^{-1}$. Despite using a high sorbent dose and low initial Se concentration, removal was not done very well. Yusof et al. [22] implement fixed-bed column for the removal of inorganic selenium species using granulated modified zeolite Y as adsorbent. After a short duration, column was saturated. Martínez et al. [23] used mineral magnetite with surface area of 0.89 $m^2\ g^{-1}$ as sorbent. 0.1 g of the solid was put in contact with 20 cm^3 of the solution, and equilibrium was reached after 30 h. Rovira et al. [24] studied on natural goethite and hematite with specific surface area of 2 and 0.38 $m^2\ g^{-1}$. Adsorbent dose was 0.1 $g\ L^{-1}$, and maximum adsorption was 0.0005 $mg\ g^{-1}$ by goethite. Equilibrium was reached after 50 h, and samples were taken filtered through 0.22 μm pore size filters. Some other methods were also implemented by researchers to remove this toxic ion from aqueous media such as wetland [25], bioreactor [26], and volatilization [27].

Most of these methods, however, have low efficiency and high operating cost. Therefore, there is a real need to develop a novel, cost-effective, and efficient method. Adsorption is one of the most promising and widely applied techniques for the removal of metal ions from wastewaters. Other separation methods, such as chromatographic column, centrifuging (add more techniques), are costly and energy consuming. On the other hand, mag-molecular process is cost-effective, efficient, and generates low volume of sludge. This process is composed of two steps: first, the adsorption of Se onto the mag-molecules surface and second, the isolation of the adsorbent by a magnetic field [28,29].

The aim of this case study is to reveal the efficiency and usefulness of adsorption process of Se particles. This research paper highlights the studies on mechanism identification of adsorption process. The authors investigated the effect of initial concentration and adsorption duration on adsorption capacity and mechanism. The mechanism was studied using several kinetic and equilibrium models. Pseudo-first-order (PS1), pseudo-second-order (PS2), and Elovich models have been applied as kinetic models. Each model has a set of logical parameters with physical or chemical mining. Comparison of obtained model's parameters could result in prediction of adsorption mechanism. Also, some equilibrium isotherms such as Langmuir, Freundlich, sips, and Fritz–Schlunder were applied for the better understanding of the surface phenomena. Kinetic and equilibrium models were related to batch process. In addition to batch, continuous process in

packed-bed column was also performed, and the results were compared together.

2. Materials and methods

2.1. Materials

Ferric chloride hexahydrate ($FeCl_3{\cdot}6H_2O$, 99% purity) and ferrous chloride tetrahydrate ($FeCl_2{\cdot}4H_2O$, 99% purity), ammonium hydroxide (25%), ethanol (99.9%), and Tetraethyl orthosilicate (TEOS) were purchased from Merck Chemical Co. 3-Aminopropyl triethoxysilane (APTES) (99% purity) was supplied by Aldrich Chemical Co. Sodium selenite pentahydrate (≥99% purity) was received from Fluka Chemical Co. All chemicals were analytic grade reagents and used without further purification. Distillated deoxygenated water was used in synthesis of adsorbent.

2.2. Fabrication of mag-molecule

At the first step, magnetite nanoparticles (MNPs) were synthesized by co-precipitation of ferrous and ferric ions according to the method described by Ranjbakhsh et al. [30] with a little modification. The method is briefly discussed here. Distillated deoxygenated water (400 mL) containing $FeCl_2{\cdot}4H_2O$ (0.02 M) and $FeCl_3{\cdot}6H_2O$ (0.04 M) was bobbled with argon gas for 30 min to remove all dissolved oxygen. Diluted ammonia (2 M) was added dropwise until black precipitate appeared and pH reached to about 11. Then solution was stirred with mechanical stirrer under argon flow for 1 h at 80˚C. The obtained magnetite was isolated with magnet and washed three times with water and ethanol. Finally, magnetite was dispersed in 200 mL ethanol and then sonicated for 20 min for the sake of well-dispersion prior to silica coating. Consequently, silica was coated on the surface of magnetite according to the Stöber process [31]. In order to functionalize the surface of nanoparticles with amine ($–NH_2$), 1 g of silica-coated nanoparticles were dispersed in solution of 50 mL ethanol and 4 mL of water. Suspension was sonicated for 20 min, followed by addition of 2 mL of ammonia (25%). Then, 0.5 mL of APTES was added to the suspension and stirred at the room temperature for 24 h, followed by particles isolation with a magnet washed three times with ethanol and water. Synthesized adsorbent was kept wet and used for adsorption after measuring amount of water. To be used in continuous process, adsorbents were dried at 80˚C and then were screened so that the range of 300–500 μm of particle size was obtained.

2.3. Mag-molecule characterization

In order to study morphological properties and agglomeration trends in the functionalized and naked nanoparticles, field emission scanning electron microscopy images were taken using Hitachi-S4160. X-ray diffraction (XRD) pattern was incorporated to calculate particles size using Scherrer's equation [32] (Eq. (1)).

$$D = \frac{K\lambda}{b\cos\theta} \tag{1}$$

where K is the shape factor which is about 0.89 for magnetite, λ is the X-ray wave length (1.540598 Å), b is the width of maximum peak at half height, and θ is the angle at which the peak appears.

The XRD patterns were obtained using 3003 SC instrument (Seifert Company of Germany). Fourier transmission infrared spectroscopy (FTIR) analysis was applied to validate the surface bonding nature of the prepared samples. Patterns were recorded using Veator 22 (Bruker Company of Germany).

2.4. Batch experiment

A laboratory set-up for this process is designed and is shown with details in Fig. 1. In summary, wastewater and mag-molecule suspension, tank1 and tank2, with a specified proportion will be sent to CSTR reactor. In this reactor, which works at optimum condition, mag-molecules adsorb the selenium ions and then the suspension passes through the magnetic filter. After satiating the magnetic filter, the magnetic field will be cut off and backwashing step will be performed. Super paramagnetic nanoparticles will easily dissociate from filter when the magnetic field is cut off. Finally, adsorbent will be regenerated and ready to use again. In this work, only first step of mag-molecule process, adsorption, is evaluated.

Batch experiments were put into practice to evaluate the adsorption capacity and to obtain the kinetic and equilibrium parameters. The mechanism and thermodynamic of adsorption were studied in previous work [33]. In order to implement the batch experiments, for each test, 30 mL of solution with the selenium concentration of 50 mg L^{-1} was prepared, and the adsorbent was contacted to solution with the dose of 1 g L^{-1}. The first essential factor in the study was contact time which was varied from 5 to 360 min to find the optimum adsorption time and also to find the kinetic parameters. In the next step, reaching the equilibrium isotherm was proposed and to achieve that initial Se concentration was varied in the range of

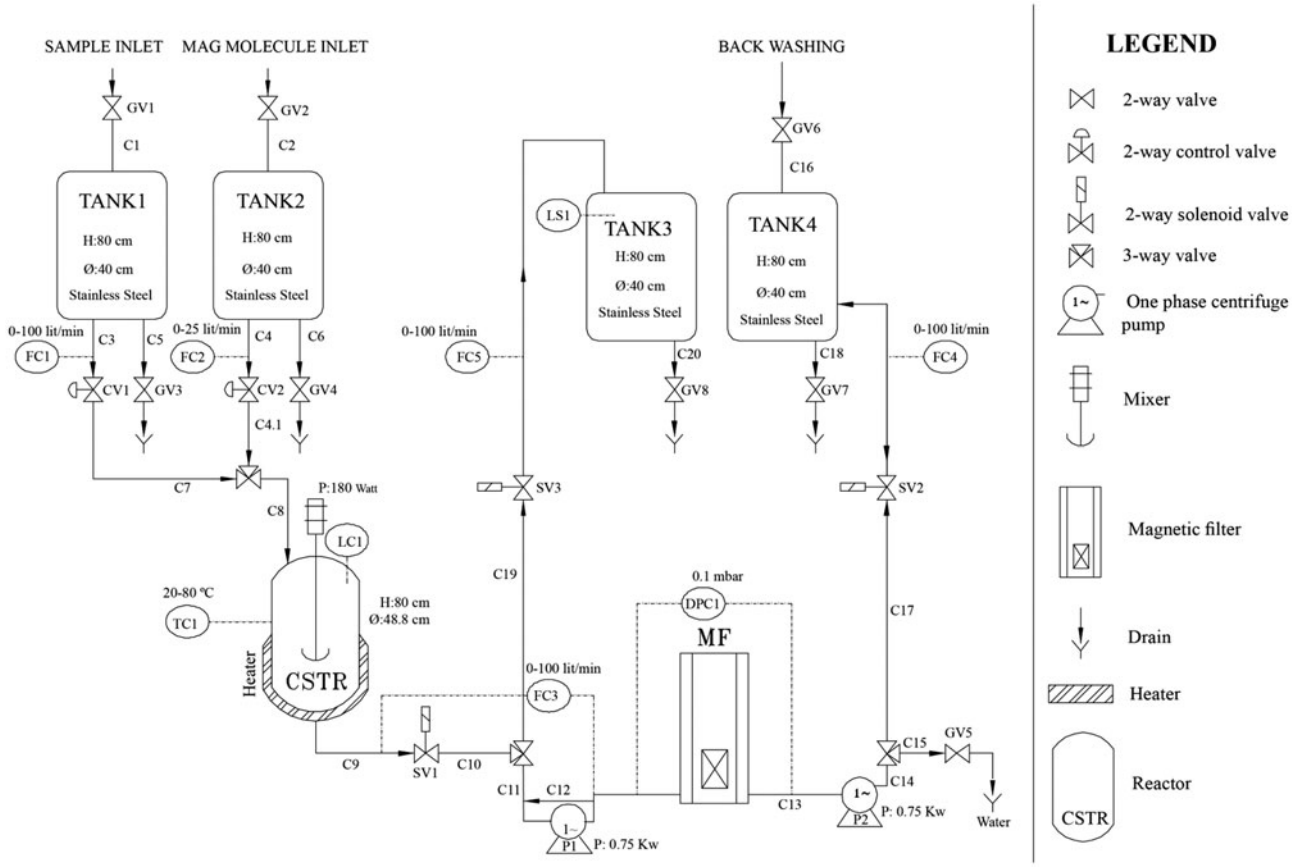

Fig. 1. Schematic diagram of mag-molecule process.

5–230 ppm. The optimum equilibrium time found in previous step was identically considered and the adsorbent dose was 1 g L^{-1}, similar to kinetic tests. Drying the synthesized adsorbent results in coagulation and consequently efficiency will decrease. So the wet adsorbent has been used in all experiments. It is necessary to find the water content of the wet adsorbent in order to reach the specific dose. One of the main factors involved in adsorption is the pH of solution. Both batch and continuous experiments were performed at room temperature and optimum pH, 2.4 for the MNPs and 1.7 for the FMNPs, which are obtained in previous work [33]. Sulfuric acid was also used as acidic agent to reach that optimum pH. A shaker with 200 rpm was used to agitation of the suspension and then an external magnetic field was exerted in order to the isolation of adsorbent from the solution. Adsorption capacity of adsorbent is calculated by the Eq. (2).

$$q_e = \frac{C_i - C_e}{M} V \tag{2}$$

where M (g) is weight of adsorbent and V (ml) is volume of solution while C_i and C_e mg L^{-1} are initial and equilibrium concentrations, respectively. Inductively coupled plasma mass spectrometry, Perkin Elmir Company Optima 7300 DV, was also applied to detect the selenium concentration in water.

2.5. Kinetic study

It is well known that there are some steps which control the adsorption process. These steps are not to be considered as simple ones. Initially, the adsorbate should pass through the media with all the limitation to reach the surface and place on it. This step consists of movement from bulk to near the surface which is facilitated by vigorous shaking at 200 rpm and causes enhancing mass transfer from bulk to near the surface. Next step is crossing-diffusing the film, thin layer near the surface, to reach the surface. After getting to the active site on the surface, a chemical reaction or a physical interaction occurs and adsorbate attaches to the surface. If the adsorbent has porous structure,

diffusion of the adsorbate through the pores could be another barrier. It is important to know how the adsorption occurs on the surface and this could be evaluated here by analyzing the obtained parameter from kinetic and isotherm models. PS1 is a primary empirical kinetic model which considers only the surface reaction [34]. The linear form of this model is given as:

$$\ln (q_e - q_t) = \ln q_e - k_1 t \tag{3}$$

In which q_t represents the adsorption capacity (mmol g^{-1}) at time t and k_1 (1 min^{-1}) is the PS1 rate constant. q_e and k_1 can be calculated from slop and intercept obtained from linear plotting of ln ($q_e - q_t$) vs. t. PS2 is also another commonly used model which has satisfactory result for the many of adsorption processes. The model predicts the mechanism of two steps which are film diffusion and then surface reaction [35]. The linear form of PS2 model is presented as:

$$\frac{t}{q_t} = \frac{1}{k_2 q_e^2} + \frac{t}{q_e} \tag{4}$$

where k_2 (g mg^{-1} min) is the PS2 rate constant. This model is able to estimate experimental q_e values quite well and usually fits the experimental data better than the PS1 model. The third applied model is the Elovich model which explains the adsorption on the heterogeneous surface [36]. The model is given as:

$$q_t = \frac{1}{B_E} \ln (1 + A_E B_E t) \tag{5}$$

In which A_E (mmol min^{-1} g^{-1}) and B_E (g $mmol^{-1}$) are the Elovich model parameters, explaining the rate of chemisorption and surface coverage, respectively.

2.6. Equilibrium study

In addition to kinetic study, equilibrium study was performed to simulate the selenium uptake by adsorbents. In this section, several isotherm models were applied for equilibrium study in order to find the relation between adsorbed component on the adsorbent surface and adsorbate amount in the fluid phase at equilibrium condition and constant temperature. The Langmuir and the Freundlich models which have two parameters are the most frequently used isotherms to fit the experiment data. Sips and Fritz–Schlunder models which have three and four parameters were also applied to find the best model for data fitting.

The Langmuir model assumptions are as follow: homogeneous surface, no interaction between adsorbed molecules, the same mechanism for all adsorption, and monolayer adsorption on the solid surface [37]. Two linear form of the Langmuir model are presented as bellow:

$$\frac{1}{q_e} = \left(\frac{1}{q_m K_L}\right)\frac{1}{C_e} + \frac{1}{q_m} \tag{6}$$

$$\frac{C_e}{q_e} = \frac{1}{q_m} C_e + \frac{1}{K_L q_m} \tag{7}$$

where q_e (mg g^{-1}) is the adsorption capacity and C_e (mg L^{-1}) is the equilibrium concentration of the adsorbate, while q_m (mg g^{-1}) is maximum capacity and K_L (L mg^{-1}) represents the energy of the adsorption.

Another widely used model is Freundlich which is the simplest empirical isotherm with assumption of a heterogeneous surface with different adsorption energy for each site. Accordingly, well-fitting of this model to equilibrium data describes the multilayer adsorption on the heterogeneous surface [38]. The linear form of the Freundlich model is given as:

$$\ln q_e = \ln K_F + \frac{1}{n_F} \ln C_e \tag{8}$$

In which K_F ((mmol g^{-1})/(L $mmol^{-1}$)^{nF}) is the model constant and n_F represents the surface heterogeneity, while they can be calculated by slope and intercept of plotting ln q_e vs. ln C_e.

Table 1
Pseudo-first-order, pseudo-second-order, and Elovich model parameters for selenium adsorption by MNPs and FMNPs

Pseudo-first order			Pseudo-second order			Elovich		
	MNPs	FMNPs		MNPs	FMNPs		MNPs	FMNPs
k_1	0.0053	0.0045	k_2	0.0034	0.0013	A_E	1.947e4	49.02
q_e	6.512	12.57	q_e	46.147	27.93	B_E	0.54	0.34
R^2	0.822	0.951	R^2	0.999	0.997	R^2	0.978	0.984
SSE	0.674	0.089	SSE	0.059	0.029	SSE	3.732	3.073

The Sips isotherm is a hybrid model which follows the Langmuir and Freundlich isotherm. At the low concentration, Sips model approaches to Freundlich while at the high concentrations, this model gives a constant value like the Langmuir isotherm [39]. The model is represented as bellow:

$$q_e = \frac{q_m (K_S C_e)^{n_S}}{1 + (K_S C_e)^{n_S}} \tag{9}$$

where K_s (L mmol^{-1}) is the affinity constant and n_S is the surface heterogeneity factor. If n_S gets a value of unity, it shows the surface is homogeneous and Sips model returns to Langmuir model. This model should be nonlinear fitted to experimental data since it has three parameters.

Fritz–Schlunder isotherm is a four-parameter empirical isotherm represented for modeling experimental data. The model is fitted with data in the nonlinear form, like the Sips model. The Fritz–Schlunder model is given as [40]:

$$q_e = \frac{q_m K_{FS} C_e^{n_{FS}}}{1 + K_{FS} C_e^{m_{FS}}} \tag{10}$$

In which n_{FS} and m_{FS} are the surface heterogeneity factors, and K_{FS} (L mmol^{-1}) is model affinity constant which corresponds to Langmuir constant (energy factor). Increasing the amount of parameter in the model gives better result for data fitting, but the parameters have less physical mining. Lack of model's physical mining cannot help to understand the mechanism of the adsorption. Therefore, two-parameter models (Langmuir and Freundlich) should be considered to understand the adsorption mechanism.

2.7. Continuous experiments

In the fixed-bed column, adsorbent is motionless and fluid containing the adsorbate move through the channels. The adsorbate moves from bulk phase to nearby of the solid surface and finally adsorbs on its surface. Considering the mentioned mechanism, mass transfer is the main factor in fixed-bed adsorption. The column performance was investigated by measuring output concentration of the adsorbate and plotting the breakthrough curve, which is normalized concentration (C_t/C_0) or volume of fluid passed the column vs. time. The experimental set-up for the column consists of a glassy column, a peristaltic pump, and a feed tank. In order to hold the adsorbent particles, glass wool has been used at the bottom of the column. The mesh size of the dry adsorbents was 300–500 μm. All experiment was performed at the laboratory condition. At the first step, the column was packed at a constant weight of adsorbent and the effect of flow rate was varied in three points. For the magnetite, flow rate of 2, 4, and 6 mL min^{-1} were examined with 2 g of adsorbent (height of 2 cm) and the column diameter was 1 cm. For the functionalized magnetite, the flow rates were 0.5, 1, and 2 mL min^{-1} and the adsorbate weight was 1 g (height of 3 cm). Lower flow rates and adsorbent's weight were chosen for functionalized magnetite, since its reaction rate is lower than naked magnetite. The initial concentration was 30 mg L^{-1} for the functionalized magnetite and 50 mg L^{-1} for the naked magnetite. The flow rates, in which the maximum adsorption capacity is obtained, were chosen as optimum value. The second step was the investigation of the effect of the bed's height which was performed by doubling the height. The optimum flow rate was fixed in previous step and the experiment was repeated in height of 4 cm (4 g) for magnetite and 6 cm (2 g) for the functionalized magnetite.

2.8. Modeling of breakthrough curve

Representing a sufficient breakthrough model could help designers to fabricate a sufficient process in the different operating conditions. There are several models to analyze the experimental data and predict the column efficiency.

The Thomas model is a simple model to study the performance of the adsorption column. This model can be derived by mass balance equation. The Thomas model assumes a second-order reaction, Langmuir model for surface adsorption at equilibrium and the condition of the non-axial dispersion [41,42]. Linear form of the model is presented as bellow:

$$\ln\left[\left(\frac{C_0}{C}\right) - 1\right] = \frac{K_{Th}\, q_0\, m}{Q} - K_{Th}\, C_0\, t \tag{11}$$

In which C and C_0 are the selenium concentration of the outlet and inlet flow, respectively. K_{Th} (1 g^{-1} min) is the Thomas rate constant, q_0 (mg g^{-1}) is the maximum adsorption capacity, M (g) is total weight of the adsorbent, and t (min) is the time. This model was nonlinear fitted to experimental data, and q_0 and K_{Th} could be calculated. These obtained parameters could be used in the condition of the same flow rate.

Another simple model is Yoon-Nelson model which focuses on the adsorption of vapors or gases in activated coal, but is frequently used for liquid systems. This model assumes that the rate of decrease in probability of adsorption for each adsorbate molecules

is proportional to the probability of adsorbate adsorption and the probability of adsorbate breakthrough on adsorbent [42,43]. The following equation represents the linear form of this model:

$$\ln\left(\frac{C}{C_0 - C}\right) = K_{YN}(t - \tau) \quad (12)$$

where K_{YN} (1 min^{-1}) is the Yoon–Nelson's proportionality constant and τ (min) is the time required for 50% adsorbate breakthrough

3. Results and discussion

3.1. Characterization of nanoparticles

3.1.1. Field emission scanning electron microscopy

Fig. 2 shows the SEM images of MNPs and FMNPs. Prepared samples were dispersed for 30 min in the ultrasonic bath. The morphology of the synthesized nanoparticles could be clearly seen. The size distribution is uniform, and synthesized nanoparticles are nearly spherical. As it could be seen in the Fig. 2, the average of particle's diameter is around 30 nm. Furthermore, dispersion of the coated particles was better than naked particles, which is likely due to fragility of silica layer and the presence of amine group on the surface of the coated nanoparticles. At first, silica layer on the surface of naked nanoparticles screens the magnetic dipolar attraction between magnetic nanoparticles, which favors the dispersion of magnetic nanoparticles in liquid media and protects them from leaching in an acidic environment. Second, due to the existence of amine groups on the silica layer, FMNPs do not attach together and prevent formation of bigger clusters [44].

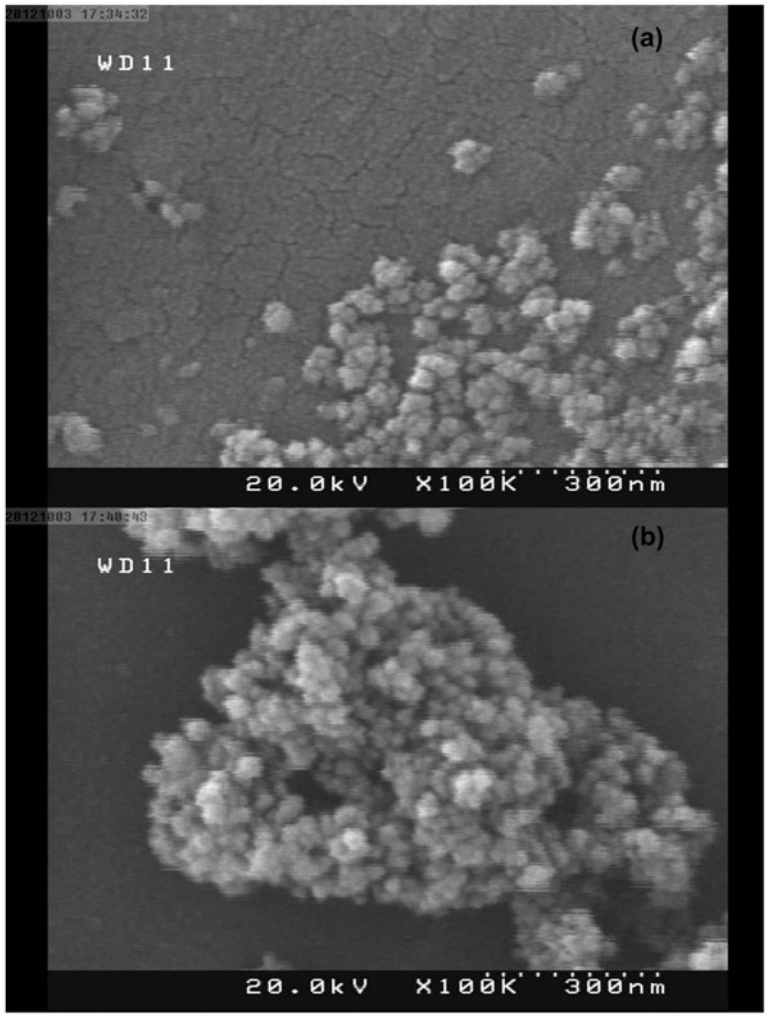

Fig. 2. SEM images of (a) FMNPs and (b) MNPs.

3.1.2. XRD Pattern

In order to check the phase purity and crystal structure of the synthesized MNPs, the XRD analysis was applied. Fig. 3 represents the XRD pattern of naked MNPs. The diffraction peaks of (220), (311), (400), (422), (511), and (440) demonstrate the fact that standard magnetite has a cubic crystal structure [32]. The obtained pattern is identical to reference pattern of JCPDS No. 19-629. According to the data obtained, average particle size has been calculated with the scherrer's equation, and was calculated to be 28.79 nm which is almost identical to observation of the SEM images.

3.1.3. Fourier transmission infrared spectroscopy

Surface nature of the synthesized nanoparticles was detected by FTIR analysis. Fig. 4 shows the FTIR spectra of naked MNPs and FMNPs. According to Fig. 4(a), there is a peak at 587 cm^{-1} which corresponds to Fe–O vibration that is related to MNPs phase. The peak at 3,440 cm^{-1} is due to stretching vibration of –OH groups at the surface of MNPs. The band at 1,635 cm^{-1} is contributed to the stretching and bending vibration of physically adsorbed H_2O on the surface. In Fig. 4(b), there is an intense and broad band appeared in 3,000–3,700 cm^{-1} region corresponding to $–NH_2$ groups which were overlapped with vibration band associated with hydroxyl groups of surface. The peak at 1,102 cm^{-1} is due to stretching vibration of Si–O–Si which demonstrates the presence of silica phase. Peaks at 2,930 and 2,859 cm^{-1} correspond to $-CH_2-$ group of APTES attached to Si, which are absent in Fig. 4(a). The band at 1,465 cm^{-1} might be due to C–H bending motion. The band at 1,640 cm^{-1} is likely due to adsorption of H_2O with the $–NH_2$ groups of surface. The presence of a peak centered at 471 cm^{-1} is probably caused by symmetric and asymmetric stretching vibration of framework and terminal Si–O groups

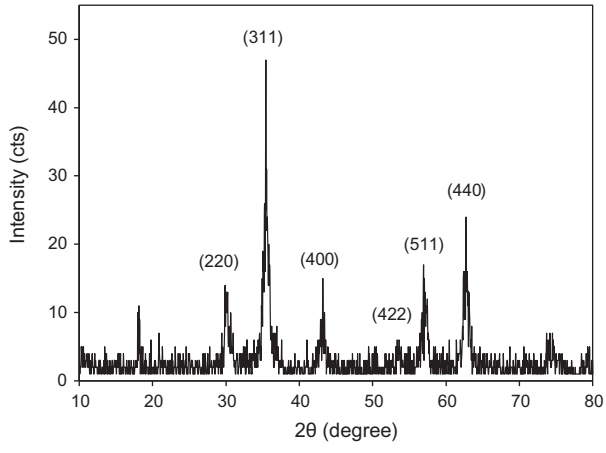

Fig. 3. XRD pattern of MNPs.

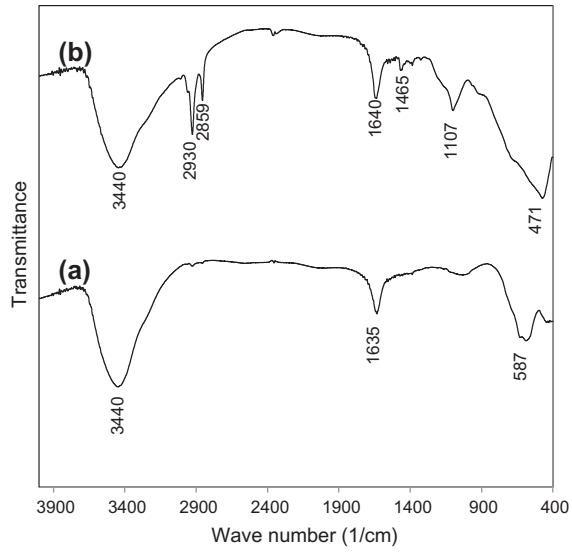

Fig. 4. FTIR spectra of (a) MNPs and (b) FMNPs.

3.2. Effect of contact time

The contact time is one of the most important processing parameters, so the adsorption capacity was calculated after 5, 10, 30, 60, 120, 180, 240, 360, and 1,020 min for two adsorbent and the result is shown in Fig. 5. At the minutes of initial, the adsorption increased rapidly so that 82% of equilibrium value was adsorbed by MNPs and 56% adsorption by FMNPs in the 10 min. Within a short period of time, adsorption rate decreased due to the occupation of active site at surface of adsorbent. For MNPs. after 1 h adsorption reached to 92% of equilibrium, whereas this quantity is 88% for FMNPs after 3 h. The result showed that the adsorption rate for MNPs is three or four time faster than FMNPs. Hence the optimum time can be proposed 1 h for MNPs and 3 h for FMNPs. However, the adsorption enhances with the time but this is not possible to increase the reaction time due to high processing cost. At the initial moments, because of vacancy of the most active site, chemical potential difference between adsorbent and solution is high, so the driving force for the mass transfer is more and consequently adsorption rate is higher. However, due to gradual and low pace growth in the adsorption capacity after 17 h, a contact time of 6 h for FMNPs and 3 h for MNPs was selected as the equilibrium time for the text equilibrium experiments.

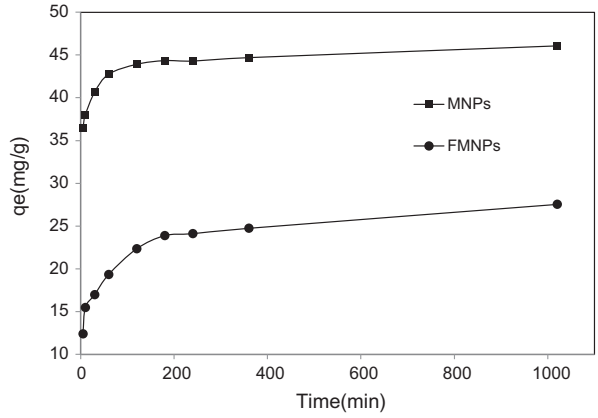

Fig. 5. Effect of reaction time on the selenium uptake by MNPs and FMNPs.

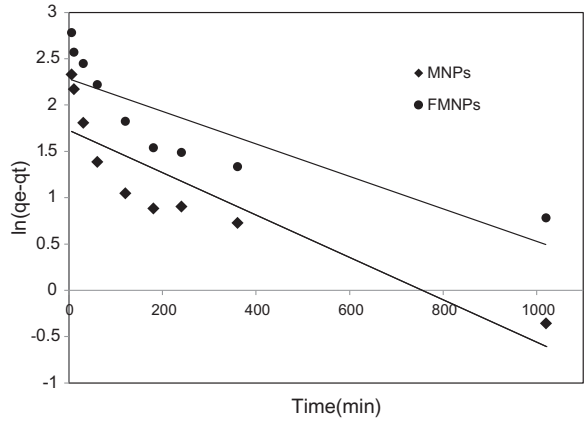

Fig. 6. Linear plot of pseudo-first-order model for MNPs and FMNPs.

3.3. Adsorption kinetics

In order to kinetic study of selenium adsorption onto adsorbent, PS1, PS2, and Elovich models were employed. The PS1 is one of the most commonly used models and predicts one-site occupancy. The PS2 is sufficient model to simulate the two-site occupancy of adsorption and was useful for different cases of adsorption. The Elovich model can divide adsorption to chemisorption and physical adsorption [36]. The calculated values for the parameters are presented in Table 1. The PS1 model is not sufficient according to the low regression coefficient and estimated equilibrium capacity for both adsorbent which has significant differences with experiments. In addition, the linear plot of PS1 model depicts deficient data fitting which is shown in Fig. 6. However, the obtained result from data fitting is showing that the PS2 model has the best conformity with the experimental data. Linear plot of this PS2 model also demonstrates this, as shown in Fig. 7. The regression coefficient is almost unity and error sum of square (SSE) for this model has less value through these three models. That can be claimed that adsorption occurs in two steps, film diffusion and surface reaction. And also, the adsorbents do not have porous structure because of conformity with PS2 model. The fitting's result with Elovich model is also represented in Table 1. Basically PS1, PS2, and intraparticle models indicate the number of limiting factor in adsorption and could be used for all the cases. On the other hand, the Elovich model should be carefully used. It is worth mentioning that the Elovich model is better to apply it for comparison cases. The regression

Table 2
The obtained parameters of isotherms for modeling of equilibrium data in selenium adsorption system

Parameters	Langmuir	Freundlich	Sips	Fritz–Schlunder
Magnetite				
q_m	33.267		88.92	71,160
K	36.85	20.8	0.02875	0.0003007
n		4.75	0.3003	0.2271
m				1.358
R^2	0.9364	0.9712	0.9789	0.9885
SSE	0.001656	0.1605	61.98	33.7
Functionalized magnetite				
q_m	28.3		34.11	363
K	0.234	7.1349	0.1266	0.02377
n		3.1665	0.5212	0.3621
m				0.7257
R^2	0.982	0.903	0.99	0.994
SSE	0.0737	0.8108	8.811	5.853

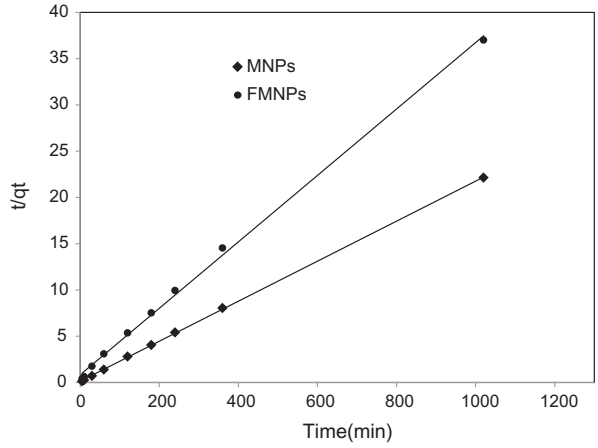

Fig. 7. Linear plot of pseudo-first-order model for MNPs and FMNPs.

coefficient and SSE indicate that this model is well fitted to experimental data. This model was nonlinear fitted to data and Fig. 8 shows a plot of Elovich equation for two series of data. The adsorption on the magnetite might occur chemically, but adsorption on the functionalized magnetite is physically. This conclusion is based on that concept of the A_E parameter which is related to chemisorption. Another logical parameter of this model is $B_{E,}$ indicating the surface coverage of the adsorbent. The calculated parameters of the model are represented in Table 1. Surface coverage value of MNPs is 0.54 and for FMNPs is 0.34, comparable with their adsorption capacity.

It could be comprehended that the adsorption of selenium occurs in two steps. The first limiting factor is the adsorbate crossing through a film near the surface which is due to the mass transfer driving force, followed by the second factor, surface reaction. The result shows that MNPs adsorb selenium chemically and FMNPs adsorb it physically. It is better to use reusable adsorbent. After adsorption, regeneration should be carried out to use refreshed adsorbent in the next cycles. It is clear that regeneration is more possible when the physical adsorption occurs. Accordingly, FMNPs are suitable adsorbent because of its reusability.

3.4. Adsorption isotherms

In order to perform equilibrium study, the initial concentration was varied from 5 to 230 mg L^{-1} and obtained isotherms are presented in Fig. 9. The adsorption capacity for both adsorbent was enhanced by growth in the ion concentration. Initial concentration is considered as a driving force for adsorption process. A rise in initial concentration though could increase the driving force and subsequently improve the adsorption efficiency. However, here the adsorption yield dwindles by increasing ion concentration so that it decreases from 99.8% at 10 mg L^{-1} to 73.7% at 50 mg L^{-1} for MNPs and decreases from 89 to 46.2% for FMNPs. This is probably due to lack of available active site at the higher concentrations. The maximum Se uptake is 52.89 mg g^{-1} for MNPs and 27.82 mg g^{-1} for FMNPs which occurred at 230 mg L^{-1} as initial concentration. As depicted in Fig. 9, the adsorption capacities did not change after 100 mg L^{-1} of initial concentration and isotherms were plateau at high solution concentration.

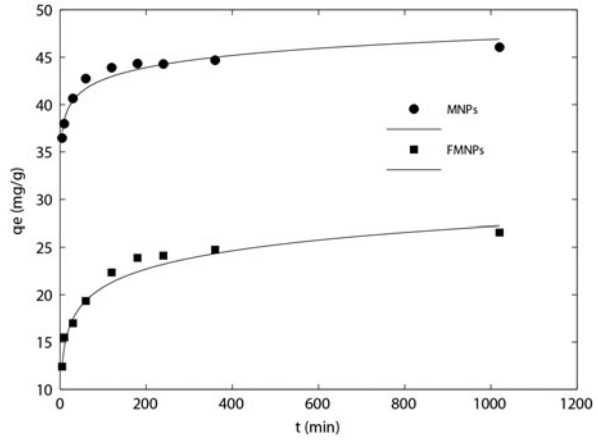

Fig. 8. Plot of the Elovich model for MNPs and FMNPs.

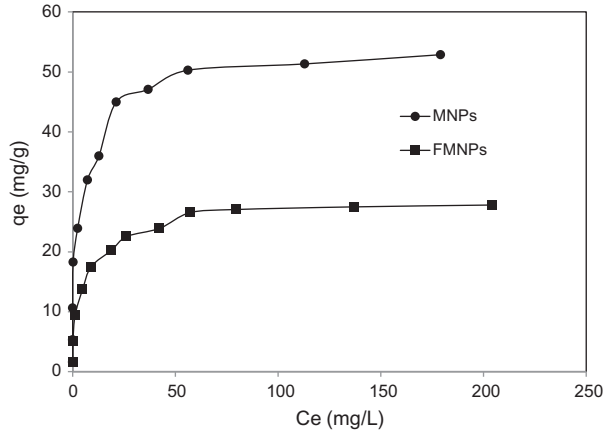

Fig. 9. Experimental isotherm obtained for selenium adsorption by for MNPs and FMNPs.

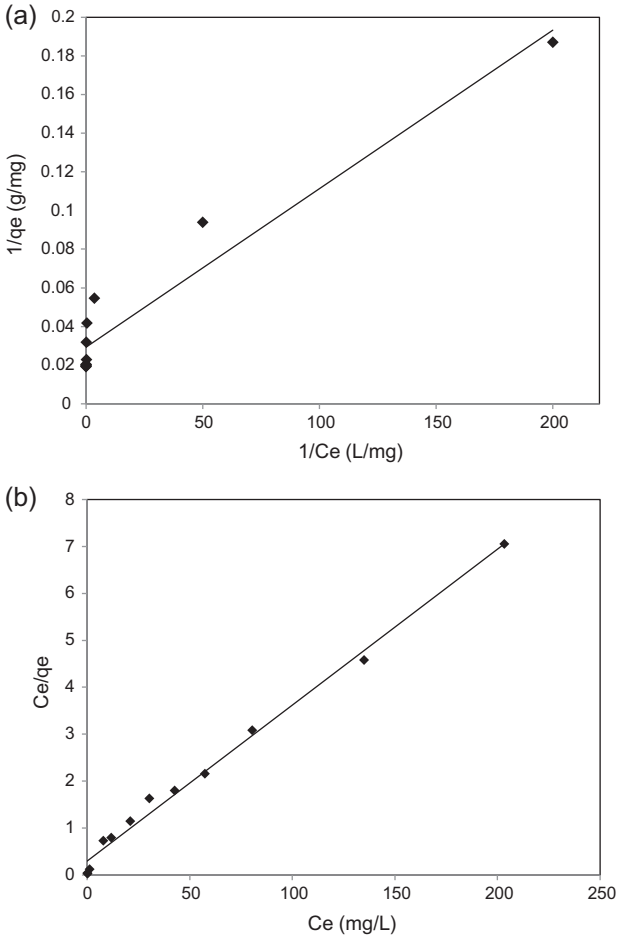

Fig. 10. Plot of linear form of Langmuir isotherm for (a) MNPs and (b) FMNPs.

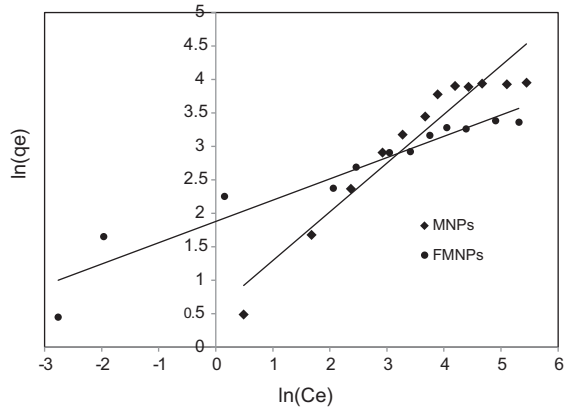

Fig. 11. Linear plot of Freundlich isotherm for MNPs and FMNPs.

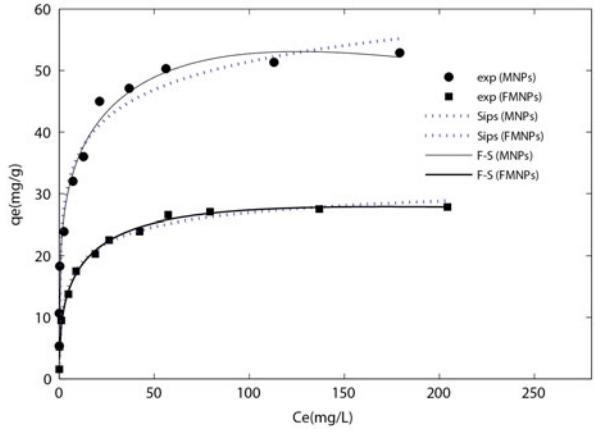

Fig. 12. Plot of Sips and Fritz–Schlunder isotherms for MNPs and FMNPs.

3.5. Application of isotherm models

Several isotherm equations were employed to model the equilibrium experiments. Langmuir and Freundlich isotherms were used in linear form and Sips and Fritz–Schlunder isotherm were nonlinear fitted to experimental data using MATLAB software. Each linear form of Langmuir equation was examined so that the best result for two kinds of sorbent could be found. Plot of C_e/q_e vs. C_e for FMNPs and $1/q_e$ vs. $1/C_e$ for MNPs is shown in Fig. 10. Plot of ln q_e vs. ln C_e for Freundlich is shown in Fig. 11 and plot of q_e vs. C_e for Sips and Fritz–Schlunder isotherms are also represented in Fig. 12. The calculated parameters of each model are represented in Table 2. Considering the calculated parameters, Freundlich for FMNPs and Langmuir for MNPs were well fitted to isotherm data, indicating that homogeneous one layer of selenium sorption occurs on FMNPs while the heterogeneous multilayer sorption occurs on the MNPs. The Fritz–Schlunder model with four parameters has the highest regression coefficient through the models, suggesting that increasing of parameter makes the model more flexible. In addition to two-parameter models, both Sips and Fritz–Schlunder models could be used for each sorbent, but the calculated parameters have significant differences with the experimental data. Maximum adsorption capacity of Sips model was obtained to be 88.92 mg g^{-1} for MNPs and 34.11 for FMNPs, while their actual values were 52.89 and 27.82 mg g^{-1}, respectively. This parameter is calculated to be 71,160 mg g^{-1} for MNPs and 363 for FMNPs by Fritz–Schlunder model.

3.6. Continuous experiments and breakthrough curves

At the first step of continuous experiments, flow rate of initial solution was examined to find the

optimum flow rate. The breakthrough curves of MNPs and FMNPs are represented in Figs. 13 and 14. As depicted in these figures, the slope of breakthrough curve grew and break time (t_b) decreased by flow rate growth. That is because of the low residence time for the adsorbate which leaves the column before equilibrium. On the other hand, increasing the flow rate led to an increment in the turbulence and consequently mass transfer was enhanced. These two factors, namely residence time and turbulence, are against each other. Bearing this in mind, optimum flow rate is the one in which the adsorbates have enough time to be adsorbed and suitable mass transfer occurs. The appropriate flow rate was obtained 4 mL min^{-1} for MNPs and 1 mL min^{-1} for FMNPs. The experimental data of column study are represented in Table 3. Second step of experiment was investigation of height effect on column performance. The columns were run at optimum flow rate and the heights were doubled. The results indicated that increment of height had a little effect on the column performance. The maximum adsorption capacity for magnetite changed from 40.58 to 42.76 mg g^{-1} and for functionalized magnetite has changed from 18.44 to 19.35 mg g^{-1}. This low increase

Table 3
Experimental data and calculated parameters of breakthrough curves for selenium uptake in fixed-bed column

Experimental parameters					
Flow rate (mL min^{-1})	Height (cm)	t_b (min)	τ_{exp} (min)	$q_{m(exp)}$ (mg g^{-1})	Adsorption percentage
Magnetite					
2	2	290	571	30.26	50.4
4	2	135	408	40.58	45.1
6	2	79	220	30.7	42.6
4	4	608	875	42.76	71.3
Functionalized magnetite					
0.5	3	613	1,013	15.05	70
1	3	214	632	18.44	57
2	3	332	272	16.48	35.8
1	6	771	1,353	18.75	71.7
Thomas model					
Flow rate (mL min^{-1})	Height (cm)	K_{Th} (1/(g min))	$q_{m(Cal)}$ (mg g^{-1})	SSE	R^2
Magnetite					
2	2	0.152	31.76	0.0088	0.981
4	2	0.202	42.36	0.0044	0.98
6	2	0.446	33.78	0.0047	0.976
4	4	0.204	41.62	0.0043	0.982
Functionalized magnetite					
0.5	3	0.217	15.13	0.0047	0.991
1	3	0.237	18.85	0.0055	0.994
2	3	0.293	17.12	0.0024	0.982
1	6	0.233	18.32	0.0112	0.992
Yoon–Nelson model					
Flow rate (mL min^{-1})	Height (cm)	K_{YN} (min^{-1})	τ_{Cal} (min)	SSE	R^2
Magnetite					
2	2	0.0075	637	1.547	0.981
4	2	0.0101	422	1.38	0.98
6	2	0.0243	235	2.914	0.965
4	4	0.0102	830	2.355	0.981
Functionalized magnetite					
0.5	3	0.0071	1,001	0.441	0.996
1	3	0.0082	627	2.344	0.971
2	3	0.0106	257	0.148	0.997
1	6	0.0078	1,234	3.939	0.977

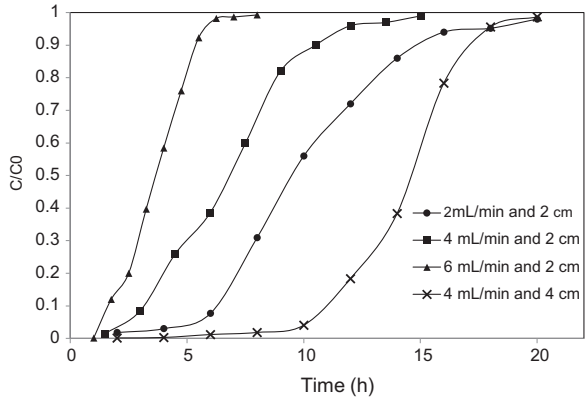

Fig. 13. The experimental breakthrough curves for selenium adsorption by magnetite in fixed-bed column, column diameter 1 cm.

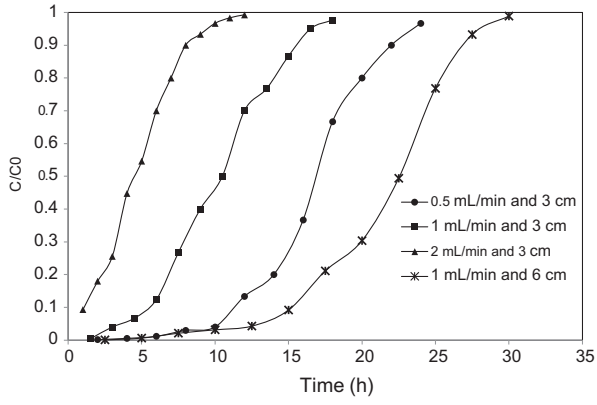

Fig. 14. The experimental breakthrough curves for selenium adsorption by functionalized magnetite in fixed-bed column, column diameter 1 cm.

in sorption capacity might be due to elongated residence time. The slope of breakthrough curves did not change by increment of column height and the break time was changed from 135 to 608 min for magnetite and 214–771 for functionalized magnetite. In the continuous system, it is better to increase the height to the extent of allowed pressure drop and the threshold of cavitation prevention.

3.7. Modeling of breakthrough curves

In order to simulate the fixed bed column, it is necessary to represent a sufficient model for breakthrough curves. For this reason, the Thomas and Yoon–Nelson equations were applied to data analysis. Both models were linear fitted by Excel software. According to the result, the Thomas model provides excellent fit to the experimental data. The obtained parameters of models are represented in Table 3 and values are comparable with experimental data. The R^2 values of the Thomas model for both adsorbent were in the range of 0.976–0.994. The absolute value for K_{Th} increased by increment of the flow rate but was rather constant by increment of bed depth. As it is obvious with reference to Table 3, the differences between calculated values and experimental data are negligible. Figs. 15 and 16 are also good evidences to the fact that the Thomas model is sufficient for prediction of breakthrough curve for this system.

Although the Thomas model is well fitted to data, the Yoon–Nelson model owns sufficient results and can be used for calculating its special parameters. The linear plot of ln $[C/(C_0 - C)]$ vs. time (t) is visible in Figs. 17 and 18 at the different initial flow rate and

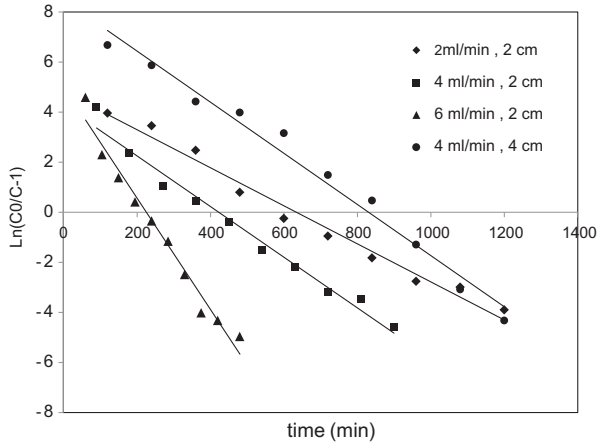

Fig. 15. Linear form of the Thomas model for breakthrough curve of selenium adsorption by magnetite, column diameter 1 cm.

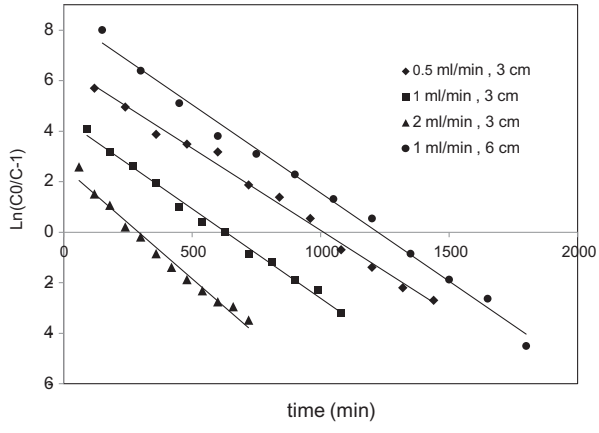

Fig. 16. Linear form of the Thomas model for breakthrough curve of selenium adsorption by functionalized magnetite, column diameter 1 cm.

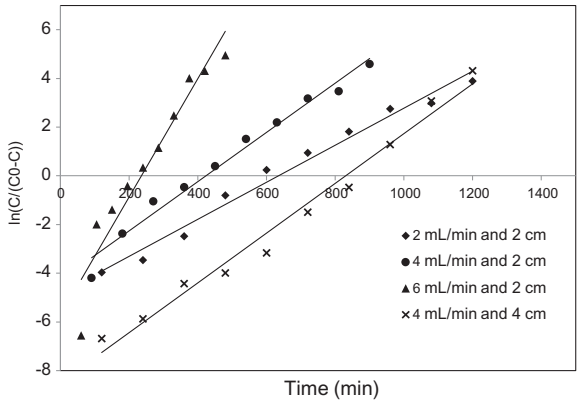

Fig. 17. Linear form of Yoon–Nelson model for breakthrough curve of selenium adsorption by functionalized magnetite, column diameter 1 cm.

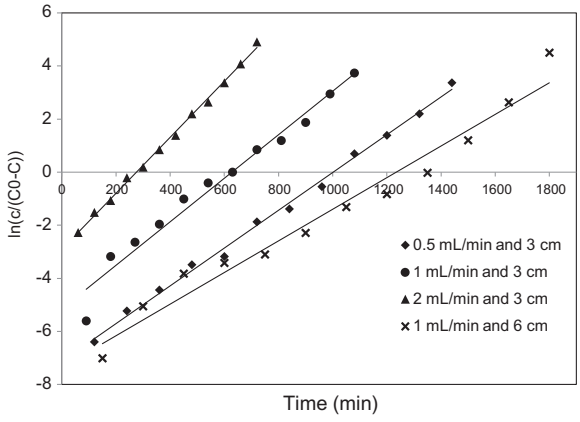

Fig. 18. Linear form of Yoon–Nelson model for breakthrough curve of selenium adsorption by functionalized magnetite, column diameter 1 cm.

the bed depth. The model was capable of being well fitted to the experimental data. The time required for 50% of adsorbate breakthrough (τ) has low differences with experiment. The linear regression coefficients for different condition were in the range of 0.965–0.997. With these explanations it could be understood that the Yoon–Nelson model fits well to experimental data. This model could be confidently used for prediction of breakthrough curve. Application of Thomas and Yoon–Nelson models depends on the parameter that is desired and if the breakthrough curve is just needed, it is better to use the Thomas model.

4. Conclusion

MNPs were synthesized and a layer of silica was coated. Prepared particles were finally functionalized with APTES. Capability of MNPs and FMNPs for selenium adsorption was investigated in batch and fixed bed-column system. The results of batch and continuous system were comparable. The results of nanoparticles characterizations were as follows:

(1) The SEM images showed that the magnetite particles are nearly spherical with about 30 nm of diameter and the functionalized particles were more dispersed.
(2) The XRD pattern has demonstrated that magnetite has cubic crystal structure and particles diameter was calculated 28.89 nm using scherrer's equation.
(3) The FTIR spectrum has exhibited the surface nature of the nanoparticles and it is found that the surface of MNPs is covered by –OH groups and FMNPs is covered by $–NH_2$.

The effect of contact time was studied on selenium adsorption onto both FMNPs and MNPs. The results have indicated that:

(1) MNPs adsorbed selenium faster than FMNPs.
(2) The MNPs has adsorbed 92% of equilibrium after 1 h while adsorption has reached 88% of equilibrium for FMNPs after 3 h.
(3) It was found that the adsorption of selenium onto both adsorbent have been controlled by pseudo-second-order mechanism. According to the result of the Elovich model.
(4) The nature of adsorption was chemically for MNPs and physically for FMNPs.
(5) The equilibrium capacity obtained 46.05 mg g^{-1} for MNPs and 27.55 mg g^{-1} for FMNPs.

The effect of initial selenium concentration was investigated and results showed that the Langmuir model for FMNPs and Freundlich model for MNPs were in agreement with experimental data. According to the concept of these models, one layer homogeneous adsorption takes place on the surface of FMNPs, while a multilayer heterogeneous adsorption occurs onto the MNPs. Three-parameter Sips and four-parameter Fritz–Schlunder isotherms were also applied and the Fritz–Schlunder was better fitted to data. These model's parameters have significant different to experimental values. These results indicate that although increasing of the number of parameters cause better fitting, the parameters lose their logical mining.

The continuous study in the fixed-bed column was performed and breakthrough curve was obtained in

three flow rates. The optimum flow rate was 4 mL min^{-1} for MNPs and 1 mL min^{-1} since maximum adsorption capacity occurs. The effect of column depth was also investigated and a change in the column performance was negligible. The Thomas model can be confidently used for simulation of breakthrough curves. The q_0 calculated from the model was much closed to measured value in the experiment. The Yoon–Nelson model was also well fitted to experimental data so can be used to predict the breakthrough curve. The application of each model depends on the desired parameter.

To conclude, the batch and continuous process in selenium adsorption by FMNPs and MNPs were studied and both systems were found to be useful. The main focus was, however, on the batch system as the mag-molecular process operates in batch or semi-batch method. Despite FMNPs have lower adsorption capacity, it could be used as adsorbent in the process because of its well dispersion capability, chemical stability, and ability to use for sequential times.

References

[1] V. Chandra, J. Park, Y. Chun, J.W. Lee, I.-C. Hwang, K.S. Kim, Water-dispersible magnetite-reduced graphene oxide composites for arsenic removal, ACS Nano 4(7) (2010) 3979–3986.

[2] L. LaConte, N. Nitin, G. Bao, Magnetic nanoparticle probes, Mater. Today 8(5) (2005) 32–38.

[3] K. Mandel, F. Hutter, C. Gellermann, G. Sextl, Synthesis and stabilisation of superparamagnetic iron oxide nanoparticle dispersions, Colloids Surf., A 390(1) (2011) 173–178.

[4] K.L. Vigor, P.G. Kyrtatos, S. Minogue, K.T. Al-Jamal, H. Kogelberg, B. Tolner, K. Kostarelos, R.H. Begent, Q.A. Pankhurst, M.F. Lythgoe, Nanoparticles functionalised with recombinant single chain Fv antibody fragments (scFv) for the magnetic resonance imaging of cancer cells, Biomaterials 31(6) (2010) 1307–1315.

[5] T. Kikumori, T. Kobayashi, M. Sawaki, T. Imai, Anti-cancer effect of hyperthermia on breast cancer by magnetite nanoparticle-loaded anti-HER2 immunoliposomes, Breast Cancer Res. Treat. 113(3) (2009) 435–441.

[6] H. Xu, Z.P. Aguilar, L. Yang, M. Kuang, H. Duan, Y. Xiong, H. Wei, A. Wang, Antibody conjugated magnetic iron oxide nanoparticles for cancer cell separation in fresh whole blood, Biomaterials 32(36) (2011) 9758–9765.

[7] P. Calvo, B. Gouritin, I. Brigger, C. Lasmezas, J.-P. Deslys, A. Williams, J.P. Andreux, D. Dormont, P. Couvreur, PEGylated polycyanoacrylate nanoparticles as vector for drug delivery in prion diseases, J. Neurosci. Methods 111(2) (2001) 151–155.

[8] E. Leo, B. Brina, F. Forni, M.A. Vandelli, In vitro evaluation of PLA nanoparticles containing a lipophilic drug in water-soluble or insoluble form, Int. J. Pharm. 278(1) (2004) 133–141.

[9] S. Kim, S.W. Bae, J.S. Lee, J. Park, Recyclable gold nanoparticle catalyst for the aerobic alcohol oxidation and C–C bond forming reaction between primary alcohols and ketones under ambient conditions, Tetrahedron 65(7) (2009) 1461–1466.

[10] O. Marin-Flores, T. Turba, C. Ellefson, K. Wang, J. Breit, J. Ahn, M.G. Norton, S. Ha, Nanoparticle molybdenum dioxide: A highly active catalyst for partial oxidation of aviation fuels, Appl. Catal., B 98(3–4) (2010) 186–192.

[11] S.K. Weber, S. Bremer, O. Trapp, Integration of reaction and separation in a micro-capillary column reactor—Palladium nanoparticle catalyzed C–C bond forming reactions, Chem. Eng. Sci. 65(7) (2010) 2410–2416.

[12] J. Baltrusaitis, J. Schuttlefield, E. Zeitler, V.H. Grassian, Carbon dioxide adsorption on oxide nanoparticle surfaces, Chem. Eng. J. 170(2–3) (2011) 471–481.

[13] D. De, S.M. Mandal, J. Bhattacharya, S. Ram, S.K. Roy, Iron oxide nanoparticle-assisted arsenic removal from aqueous system, J. Environ. Sci. Health. Part A Environ. Sci. Health 44(2) (2009) 155–162.

[14] P.I. Girginova, A.L. Daniel-da-Silva, C.B. Lopes, P. Figueira, M. Otero, V.S. Amaral, E. Pereira, T. Trindade, Silica coated magnetite particles for magnetic removal of Hg 2+ from water, J. Colloid Interface Sci. 345(2) (2010) 234–240.

[15] N.M. Mahmoodi, S. Khorramfar, F. Najafi, Amine-functionalized silica nanoparticle: Preparation, characterization and anionic dye removal ability, Desalination 279(1–3) (2011) 61–68.

[16] P. Panneerselvam, N. Morad, K.A. Tan, Magnetic nanoparticle (Fe_3O_4) impregnated onto tea waste for the removal of nickel (II) from aqueous solution, J. Hazard. Mater. 186(1) (2011) 160–168.

[17] O. Levander, R. Burk, Update of human dietary standards for selenium, in: D.L. Hatfield, M.J. Berry, V.N. Gladyshev (Eds.), Selenium, Springer, New York, NY, 2006, pp. 399–410, doi:10.1007/0-387-33827-6_35.

[18] M.P. Rayman, The importance of selenium to human health, Lancet 356(9225) (2000) 233–241.

[19] G. Jörg, R. Bühnemann, S. Hollas, N. Kivel, K. Kossert, S. Van Winckel, C.L. Gostomski, Preparation of radiochemically pure ^{79}Se and highly precise determination of its half-life, Appl. Radiat. Isot. 68(12) (2010) 2339–2351.

[20] K.L. Wasewar, B. Prasad, S. Gulipalli, Removal of selenium by adsorption onto granular activated carbon (GAC) and powdered activated carbon (PAC), CLEAN—Soil Air Water 37(11) (2009) 872–883.

[21] X. Meng, S. Bang, G.P. Korfiatis, Removal of selenocyanate from water using elemental iron, Water Res. 36(15) (2002) 3867–3873.

[22] A. Yusof, N. Idris, N.A. Malek, A.K. Wood, Use of granulated modified zeolite Y for the removal of inorganic arsenic and selenium species, J. Radioanal. Nucl. Chem. 281(2) (2009) 269–272.

[23] M. Martínez, J. Giménez, J. de Pablo, M. Rovira, L. Duro, Sorption of selenium(IV) and selenium(VI) onto magnetite, Appl. Surf. Sci. 252(10) (2006) 3767–3773.

[24] M. Rovira, J. Giménez, M. Martínez, X. Martínez-Lladó, J. de Pablo, V. Martí, L. Duro, Sorption of selenium(IV) and selenium(VI) onto natural iron oxides: Goethite and hematite, J. Hazard. Mater. 150(2) (2008) 279–284.

[25] D. Hansen, P.J. Duda, A. Zayed, N. Terry, Selenium removal by constructed wetlands: Role of biological volatilization, Environ. Sci. Technol. 32(5) (1998) 591–597.
[26] S. Soda, M. Kashiwa, T. Kagami, M. Kuroda, M. Yamashita, M. Ike, Laboratory-scale bioreactors for soluble selenium removal from selenium refinery wastewater using anaerobic sludge, Desalination 279 (1–3) (2011) 433–438.
[27] E. Pilon-Smits, M. De Souza, C. Lytle, C. Shang, T. Lugo, N. Terry, Selenium volatilization and assimilation by hybrid poplar (Populus tremula x alba), J. Exp. Bot. 49(328) (1998) 1889–1892.
[28] D. Kim, Y. Zhang, W. Voit, K. Rao, M. Muhammed, Synthesis and characterization of surfactant-coated superparamagnetic monodispersed iron oxide nanoparticles, J. Magn. Magn. Mater. 225(1–2) (2001) 30–36.
[29] J. Watson, Magnetic filtration, J. Appl. Phys. 44(9) (1973) 4209–4213.
[30] E. Ranjbakhsh, A. Bordbar, M. Abbasi, A. Khosropour, E.S. Soolari, Enhancement of stability and catalytic activity of immobilized lipase on silica-coated modified magnetite nanoparticles, Chem. Eng. J. 179 (2012) 272–276.
[31] Z. Lei, X. Pang, N. Li, L. Lin, Y. Li, A novel two-step modifying process for preparation of chitosan-coated Fe_3O_4/SiO_2 microspheres, J. Mater. Process. Technol. 209(7) (2009) 3218–3225.
[32] H. Itoh, T. Sugimoto, Systematic control of size, shape, structure, and magnetic properties of uniform magnetite and maghemite particles, J. Colloid Interface Sci. 265(2) (2003) 283–295.
[33] Y.N. Larimi, M.H. Mallah, M.A. Moosavian, J. Safdari, Fabrication of a magmolecule using nanoparticle and evaluation of its adsorption capacity for selenium ions from nuclear wastewater, J. Radioanal. Nucl. Chem. 298(3) (2013) 1511–1518.
[34] E. Repo, J.K. Warchol, T.A. Kurniawan, M.E. Sillanpää, Adsorption of Co(II) and Ni(II) by EDTA- and/or DTPA-modified chitosan: Kinetic and equilibrium modeling, Chem. Eng. J. 161(1–2) (2010) 73–82.
[35] Y.-M. Hao, C. Man, Z.-B. Hu, Effective removal of Cu (II) ions from aqueous solution by amino-functionalized magnetic nanoparticles, J. Hazard. Mater. 184 (1–3) (2010) 392–399.
[36] C. Cheung, J. Porter, G. Mckay, Sorption kinetic analysis for the removal of cadmium ions from effluents using bone char, Water Res. 35(3) (2001) 605–612.
[37] Y. Vijaya, S.R. Popuri, V.M. Boddu, A. Krishnaiah, Modified chitosan and calcium alginate biopolymer sorbents for removal of nickel (II) through adsorption, Carbohydr. Polym. 72(2) (2008) 261–271.
[38] Y. Ho, J. Porter, G. McKay, Equilibrium isotherm studies for the sorption of divalent metal ions onto peat: Copper, nickel and lead single component systems, Water Air Soil Pollut. 141(1–4) (2002) 1–33.
[39] Y. Liu, Y.-J. Liu, Biosorption isotherms, kinetics and thermodynamics, Sep. Purif. Technol. 61(3) (2008) 229–242.
[40] S. Basha, Z. Murthy, B. Jha, Sorption of Hg (II) from aqueous solutions onto Carica papaya: Application of isotherms, Ind. Eng. Chem. Res. 47(3) (2008) 980–986.
[41] M. Calero, F. Hernáinz, G. Blázquez, G. Tenorio, M. Martín-Lara, Study of Cr (III) biosorption in a fixed-bed column, J. Hazard. Mater. 171(1-3) (2009) 886–893.
[42] S. Kundu, A. Gupta, As(III) removal from aqueous medium in fixed bed using iron oxide-coated cement (IOCC): Experimental and modeling studies, Chem. Eng. J. 129(1–3) (2007) 123–131.
[43] S. Baral, N. Das, T. Ramulu, S. Sahoo, S. Das, G.R. Chaudhury, Removal of Cr(VI) by thermally activated weed *Salvinia cucullata* in a fixed-bed column, J. Hazard. Mater. 161(2–3) (2009) 1427–1435.
[44] Y.-H. Deng, C.-C. Wang, J.-H. Hu, W.-L. Yang, S.-K. Fu, Investigation of formation of silica-coated magnetite nanoparticles via sol–gel approach, Colloids Surf., A 262(1–3) (2005) 87–93.